MOLECULAR AND CELLULAR BIOLOGY, Jan. 2009, p. 229–240 Vol. 29, No. 1
0270-7306/09/$08.00+0 doi:10.1128/MCB.01400-08

Pot1b Deletion and Telomerase Haploinsufficiency in Mice Initiate an ATR-Dependent DNA Damage Response and Elicit Phenotypes Resembling Dyskeratosis Congenita▽†

Hua He,[1] Yang Wang,[1] Xiaolan Guo,[1] Sonal Ramchandani,[1] Jin Ma,[1] Mei-Feng Shen,[1] Dennis A. Garcia,[2] Yibin Deng,[1] Asha S. Multani,[1] Mingjian James You,[3] and Sandy Chang[1,3]*

Department of Genetics[1] and Department of Hematopathology,[3] Box 1010, The M. D. Anderson Cancer Center, 1515 Holcombe Boulevard, Houston, Texas 77030, and University of Houston Downtown, One Main Street, Houston, Texas 77002[2]

Received 5 September 2008/Returned for modification 25 September 2008/Accepted 7 October 2008

The Protection of telomeres 1 (POT1) protein is a single-stranded telomere binding protein that is essential for proper maintenance of telomere length. Disruption of POT1 function leads to chromosome instability and loss of cellular viability. Here, we show that targeted deletion of the mouse *Pot1b* gene results in increased apoptosis in highly proliferative tissues. In the setting of telomerase haploinsufficiency, loss of *Pot1b* results in depletion of germ cells and complete bone marrow failure due to increased apoptosis, culminating in premature death. *Pot1b*$^{-/-}$ *mTR*$^{+/-}$ hematopoietic progenitor and stem cells display markedly reduced survival potential in vitro. Accelerated telomere shortening, increased G overhang and elevated number of chromosome end-to-end fusions that initiate an ATR-dependent DNA damage response were also observed. These results indicate an essential role for *Pot1b* in the maintenance of genome integrity and the long-term viability of proliferative tissues in the setting of telomerase deficiency. Interestingly, these phenotypes closely resemble those found in the human disease dyskeratosis congenita (DC), an inherited syndrome characterized by bone marrow failure, hyperpigmentation, and nail dystrophy. We anticipate that this mouse will serve as a useful model to further understand the pathophysiology of DC.

Telomeres are protein-DNA complexes that cap the ends of most eukaryotic chromosomes and maintain genomic stability by providing both end protection and a mechanism for maintenance of chromosomal ends. Mammalian telomeres consist of TTAGGG repetitive sequences that terminate in a 3′ single-stranded G-rich overhang that can be sequestered into a lariat-like structure termed the T-loop. This structure likely serves to protect chromosome termini from being recognized as double-strand breaks that would otherwise activate DNA damage checkpoint responses or participate in aberrant recombination events (26). In most eukaryotes, telomeres are maintained by the enzyme telomerase, a specialized reverse transcriptase that adds telomeric DNA to the 3′ ends of telomeres. Telomerase is limiting in human somatic cells, leading to telomere attrition with each round of DNA replication, and eventually critically shortened telomeres are generated that engage canonical DNA damage response pathways to initiate the onset of apoptosis or replicative senescence depending on cell type (9). In the absence of telomerase, mice show progressive telomere shortening with successive intercrosses (4). While early-generation telomerase knockout mice do not display overt phenotypes, late-generation mice with critically shortened telomeres display increased apoptosis, cytogenetic abnormalities, and cellular defects in highly proliferative compartments, including the hematopoietic and reproductive systems (19). These results strongly support the view that the long-term homeostasis of renewing organ systems depends upon telomerase-mediated maintenance of telomere length and function.

The T-loop is bound by the shelterin complex of six core proteins composed of TRF1, TRF2, RAP1, TIN2, TPP1, and POT1, which serve to protect telomeres from undergoing inappropriate repair by the nonhomologous end joining and homologous recombination pathways (26). POT1 was originally discovered in *Schizosaccharomyces pombe* by its sequence similarity to the α subunit of telomere binding protein TEBPα/β (2) and is the only protein in the complex that binds the single-stranded 3′ G-rich overhang. POT1 forms a heterodimer with TPP1, which in turn connects POT1 with TIN2 and TRF1/TRF2. POT1 homologs have been identified in a large variety of eukaryotes, including plant (30), *Caenorhabditis elegans* (27), chicken (38), mice (14, 16, 41), and human (3, 23). All POT1 proteins contain two highly conserved oligonucleotide/oligosaccharide binding folds that interact with single-stranded telomeric DNA with high affinity (2, 3, 14, 20, 23, 27, 41). Biochemical analyses revealed that POT1 negatively regulates telomerase activity in vitro by binding to and limiting telomerase access to the terminal G residue of telomeres (18, 21). When bound to TPP1, POT1 can also localize to a more internal position on the 3′ overhang to facilitate telomerase activity and telomere elongation (37, 42). These results suggest that POT1 could function as both a negative and a positive regulator of telomere length, depending on how it competes with telomerase for access to the 3′ overhang.

The rodent genome encodes two highly similar POT1 pro-

* Corresponding author. Mailing address: Department of Genetics, Box 1006, The M. D. Anderson Cancer Center, 1515 Holcombe Blvd., Houston, TX 77030. Phone: (713) 834-6361. Fax: (703) 834-6363. E-mail: schang@mdanderson.org.

† Supplemental material for this article may be found at http://mcb.asm.org/.

▽ Published ahead of print on 20 October 2008.

teins, Pot1a and Pot1b, while other mammalian genomes possess only one POT1 gene (14, 16, 41). While both Pot1a and Pot1b are required to fully protect telomeres from initiating a DNA damage response (DDR), these two proteins also possess distinct functions. Deletion of *Pot1a* in mice results in early embryonic lethality, increased cytogenetic abnormalities, and activation of an ATR-dependent DDR at telomeres, initiating both nonhomologous end joining and homologous recombination-dependent repair pathways (7, 8, 12, 16, 41). Deletion of *Pot1b*, however, does not elicit a robust DDR at telomeres. Rather, elongation of the 3′ G overhang is observed (16). These results suggest that Pot1a is primarily required to protect telomeres from an ATR-dependent DNA damage checkpoint emanating from the single-stranded overhang, while Pot1b appears to be required for formation of the 3′ overhang.

To elucidate the function of Pot1b in vivo, we generated a conditional *Pot1b* knockout mouse. Deletion of the *Pot1b* gene results in increased apoptosis in highly proliferative tissues, including complete bone marrow failure and premature death. These results indicate a role for Pot1b in the maintenance of genome integrity and long-term tissue viability. Interestingly, the phenotypes observed in $Pot1b^{-/-}$ $mTR^{+/-}$ mice closely resemble those found in the human disease dyskeratosis congenita (DC), an inherited syndrome characterized by bone marrow failure, hyperpigmentation, and nail dystrophy. The generation of a faithful mouse model of DC should permit mechanistic insights into this disease process and serve as a platform to test and validate future therapeutics.

MATERIALS AND METHODS

Generation of *Pot1b* conditional knockout mouse and cell lines. A bacterial artificial chromosome encoding the entire *Pot1b* gene was isolated from an RPCI-22 129SvJ bacterial artificial chromosome genomic library (Children's Hospital, Oakland Research Institute). A long-range, high-fidelity PCR strategy was used to obtain the correct genomic fragments for use in generating the targeting construct. The *Pot1b* targeting vector was generated by subcloning a 2.8-kb EcoRI-XhoI fragment 5′ of the first *loxP* site in the pKOII vector, which included a PGK *neo* cassette flanked by *frt* sites and a negative selection (diphtheria toxin) cassette. A 11.2-kb SacII-NotI fragment containing exons 3 and 4 was subcloned 3′ of the *neo* cassette, and a second *loxP* site was inserted 3′ of exon 5. The vector was linearized with NotI, and gene targeting into TC1 embryonic stem (ES) cells was performed according to standard techniques. ES cells containing the correct recombination events were identified by Southern analysis and karyotyped, and two clones were selected for injection into C57BL/6 blastocysts. Chimeric mice were crossed with ZP3-Cre animals to generate $Pot1b^{+/-}$ mice, and these were intercrossed to generate $Pot1b^{-/-}$ mice. $Pot1b^{-/-}$ mice were bred with $mTR^{-/-}$ mice (mice deficient in telomerase RNA) to generate $Pot1b^{+/-}$ $mTR^{+/-}$ mice, and these were intercrossed to generate the cohort. $Pot1b^{-/-}$ $mTR^{+/-}$ and $Pot1b^{+/-}$ $mTR^{-/-}$ mice were also crossed to generate additional $Pot1b^{-/-}$ $mTR^{-/-}$ mice. All mice were maintained in a C57BL/6 129Sv mixed genetic background. Primary mouse embryonic fibroblasts (MEFs) were prepared from individual day 13.5 embryos derived from mice and cultured under 3% oxygen. Passage 2 primary MEFs were immortalized with pBabeSV40LT.

Histology, immunohistochemistry, and TUNEL assays. Tissues were fixed in 10% formalin, paraffin embedded, sectioned at a 5-um thickness, and stained for hematoxylin and eosin. For immunohistochemistry, antigens were retrieved using 10 mM citrate buffer, pH 6.0, for 15 min. The following primary antibodies were used: p21 (sc-6246; Santa Cruz) at 1:50 and p53 (NCL-p53-CM5p; Novocastra) at 1:500. Sections were incubated with the following: biotinylated rabbit anti-mouse F(ab)′ (Accurate Chemical) at a 1:250 dilution (for p21), Envision Plus-labeled polymer, and anti-rabbit horseradish peroxidase-conjugated antibody (Dako) (for p53). Immunoreactivity was revealed using diaminobenzidine (DAB) (Dako). A terminal deoxynucleotidyltransferase-mediated dUTP-biotin nick end labeling (TUNEL) assay was performed with an ApopTag Plus Peroxidase In Situ Apoptosis Detection Kit (Chemicon) according to the manufacturer's instructions. Slides were subsequently counterstained in Fast Red for 1 min, dehydrated through an ethanol series to xylene, and mounted under glass coverslips in Permount (Fisher).

shRNA interference and antibodies. RNA was isolated from approximately 10^6 cells with a Qiagen RNAeasy kit. Reverse transcription-PCR (RT-PCR) was performed with an oligo(dT) RT-PCR system according to manufacturer's protocol (Invitrogen). Two short hairpin RNAs (shRNAs) against murine Pot1b (shPot1b) were generated in pSuper as described previously (14). The following antibodies were used: phospho-p53 Ser15 (9284) and p21 (Sc-6246) from Santa Cruz, γ-tubulin from Sigma, phospho-ATR (2853S) from Cell Signaling, and γ-H2AX (05-636) from Upstate.

Flow cytometry. BD Pharmingen's Annexin V-PE Apoptosis Detection Kit was used to quantitatively determine the percentage of cells that are actively undergoing apoptosis within nucleated blood cells. After processing by red blood cell (RBC) lysis buffer, 1×10^5 cells were incubated at room temperature in a 100-μl volume of 1× binding buffer with annexin V-phycoerythrin and 7-aminoactinomycin D (7-AAD) for 15 min; then an additional 400 μl of buffer was added for direct analysis. For analysis of lineage markers, cells (1×10^6) in a 100-μl volume were incubated at 4°C for 30 min in phosphate-buffered saline (PBS) containing 2% bovine serum albumin with monoclonal antibodies against Gr-1, CD11b, B220, CD3, c-Kit, Sca-1, or their isotype controls (Caltag). The cells were then washed with PBS containing 2% bovine serum albumin, fixed with 1% formaldehyde in PBS, and applied for analysis on a FACSCalibur (Becton Dickinson) fluorescence-activated cell sorter (FACS).

Colony-forming assay. A total of 2×10^4 bone marrow cells were plated in a 35-mm diameter dish containing MethoCult medium (StemCell Technologies, Canada) following the manufacturer's instructions. Colonies were counted on day 8.

Telomere length and G-strand overhang assays. In gel hybridization with a γ-^{32}P-C_3TA_2 oligonucleotide and subsequent denaturation and hybridization with a γ-^{32}P-T_2AG_3 oligonucleotide were performed as described previously (4).

Cytogenetics analysis and quantitative FISH. Metaphase chromosomes from MEFs, splenocytes, and bone marrow (BM) were prepared 1 to 4 h after colcemide treatment, as previously described (41), and subjected to Giemsa staining and/or fluorescence in situ hybridization (FISH) with Cy3-labeled T_2AG_3 peptide-nucleic acid (PNA) probe as described previously (41). Images were captured on a Nikon Eclipse 800 microscope. Depending on the quality of metaphase spreads, 20 to 40 metaphases from each sample were analyzed in detail. Quantitative telomere FISH was performed using the microscopy system described above with a 14-bit cooled charge-coupled-device camera and the Metamorph image acquisition software. Images were dark subtracted and flat fielded prior to quantitative analysis in a blinded manner.

RESULTS

Generation of a conditional *Pot1b* knockout mouse. The *Pot1b* gene encodes 16 exons, with exon 3 containing the translation initiation site and exon 4 containing a portion of the oligonucleotide/oligosaccharide binding domain critically important for telomere binding (14). We generated a conditional *Pot1b* knockout construct in which both exons 3 and 4 were flanked by *loxP* sites. Excision of these exons by Cre recombinase is predicted to generate an in-frame termination codon, enabling conditional *Pot1b* inactivation (Fig. 1A). Electroporation of this construct into ES cells and selection for G418-resistant clones yielded six correctly recombined (*rec*) ES cell lines, as determined by genomic Southern analysis (Fig. 1B). Two $Pot1b^{rec/+}$ ES cell lines were injected into blastocysts to generate chimeric mice, and crosses between chrimeric mice and the ZP3-Cre deleter mice (22) produced $Pot1b^{+/-}$ mice. Crossing $Pot1b^{+/-}$ mice generated $Pot1b^{-/-}$ MEFs. RT-PCR of mRNA isolated from these MEFs did not detect any transcripts encoding truncated *Pot1b* (Fig. 1C), suggesting that we generated a *Pot1b* null allele. Unlike the early embryonic lethal phenotype observed in *Pot1a* knockouts (41), $Pot1b^{-/-}$ mice are viable and fertile (Fig. 1D).

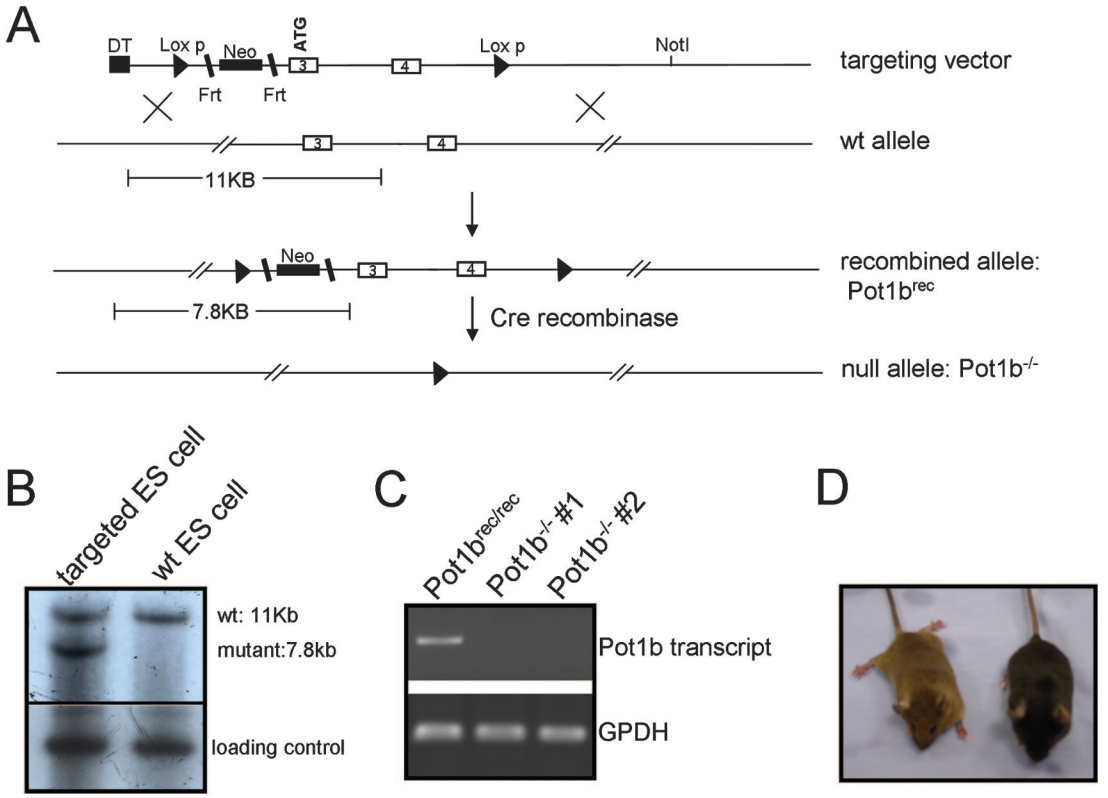

FIG. 1. Conditional deletion of mouse *Pot1b*. (A) Schematic depicting the conditional *Pot1b* knockout construct, showing exons 3 and 4 flanked by *loxP* sites (arrowheads) and the neomycin gene (black rectangle) flanked by Frt sites (slanted bars). The diphtheria toxin (DT) negative selection marker is indicated. Also shown are the *Pot1b* locus, the recombined ($Pot1b^{rec}$) allele, and the null ($Pot1b^{-/-}$) allele. (B) Correct targeting into ES cells is expected to yield two fragments of 11 and 7.8 kb after BglI digestion, which are detected with a 5′ probe. (C) RT-PCR of *Pot1b* transcripts from total RNAs isolated from MEFs of the indicated genotypes. Glyceraldehyde-3-phosphate dehydrogenase (GPDH) is included as loading control. (D) Pot1b null mice are viable.

Deletion of *Pot1b* results in cell death in highly proliferative organs. $Pot1b^{-/-}$ mice appear grossly normal although both sexes are smaller than wild type (wt) littermate controls (see Fig. S1 in the supplemental material). Matings with wt female mice revealed that $Pot1b^{-/-}$ males became sterile after producing only three to four litters (see Fig. S2A in the supplemental material). Because reproductive function is highly dependent on the development and proliferation of germ cells, we analyzed testes derived from $Pot1b^{-/-}$ males. Gross inspection revealed that by 220 days of age, the sizes of $Pot1b^{-/-}$ testes were reduced by approximately twofold compared with those from age-matched wt or $Pot1b^{+/-}$ controls, whereas all other organs examined, including spleen, were proportional to body size (see Fig. S2B and C in the supplemental material; also data not shown). Histological analyses revealed that in contrast to age-matched wt controls, all $Pot1b^{-/-}$ testes displayed a striking absence of spermatogenesis in ~60% of seminiferous tubules, which correlated with a ~20-fold increase in apoptosis, as revealed by TUNEL assay (Fig. 2A and B). However, the less proliferative Sertoli and Leydig support cells appeared largely unaffected. $Pot1b^{-/-}$ mice also displayed a ~15-fold increase in apoptotic cells concentrated around the highly proliferative intestinal crypt epithelia, confirmed by TUNEL staining (Fig. 2A and C). These results suggest that proliferative cells of the testes and intestine require functional Pot1b to prevent the onset of apoptosis.

Generation of $Pot1b^{-/-}$ mice with telomerase deficiency. The testicular and intestinal phenotypes are reminiscent of those observed in late-generation telomerase knockout mouse, in which germ cell depletion and intestinal apoptosis are prominent features as a result of decreased telomere length (19, 28, 40). We have shown previously that Pot1b functionally interacts with TPP1 (12, 14). Since the POT1-TPP1 heterodimer recruits telomerase to telomeric ends (37, 42), we postulated that in the absence of Pot1b, diminished recruitment of telomerase to telomeres might result in accelerated telomere shortening, thereby exacerbating the phenotypes observed in the $Pot1b^{-/-}$ mice. To test this hypothesis, we intercrossed $Pot1b^{-/-}$ mice with telomerase-null first-generation $mTR^{-/-}$ mice to generate $Pot1b^{+/-}$ $mTR^{+/-}$ mice. We then intercrossed double-heterozygous animals to generate wt, $Pot1b^{-/-}$ $mTR^{+/+}$, $Pot1b^{-/-}$ $mTR^{+/-}$, and $Pot1b^{-/-}$ $mTR^{-/-}$ mice (see Fig. S2D in the supplemental material). In some experiments, $Pot1b^{+/-}$ $mTR^{+/-}$ mice (indistinguishable from wt mice in all of our phenotypic analyses) were used as controls. All genotypes were produced at Mendelian frequencies except for the $Pot1b^{-/-}$ $mTR^{-/-}$ genotype, which was underrepresented (only 1 out of 90 offspring; expected number, ~6). Intercross-

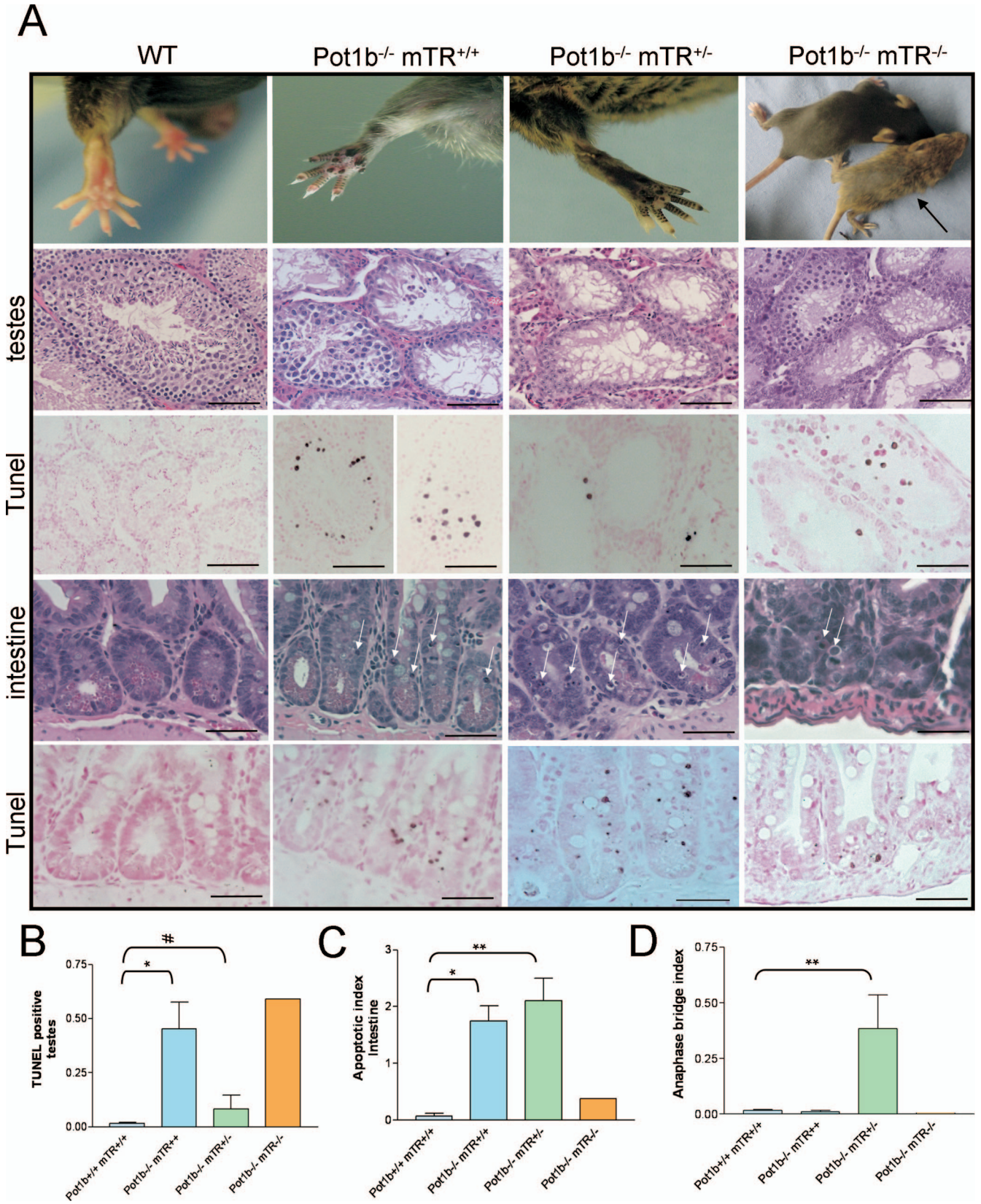

FIG. 2. Effect of *Pot1b* deletion on mouse phenotypes. (A, first row) Hyperpigmentation of paws of *Pot1b*$^{-/-}$ *mTR*$^{+/+}$ (age, 203 days) and *Pot1b*$^{-/-}$*mTR*$^{+/-}$ (189 days) mice but not wt (308 days) mice. The last panel shows a runted 12-day old *Pot1b*$^{-/-}$ *mTR*$^{-/-}$ mouse (arrow) next to a *Pot1b*$^{+/-}$ *mTR*$^{+/-}$ littermate control. (Second row) Hematoxylin and eosin staining of sections of testes of the indicated genotypes. Ages of all mice are as above. (Third row) TUNEL staining

ing *Pot1b*$^{+/-}$ *mTR*$^{-/-}$ mice yielded four male *Pot1b*$^{-/-}$ *mTR*$^{-/-}$ mice in the expected Mendelian ratio (see Fig. S2E in the supplemental material). However, except for one mouse that lived for 13 days, all *Pot1b*$^{-/-}$ *mTR*$^{-/-}$ pups died within days after birth. These results suggest that in the absence of telomerase, deletion of *Pot1b* is incompatible with long-term survival.

Telomerase deficiency enhanced cellular defects observed in *Pot1b*$^{-/-}$ mice. Although *Pot1b*$^{-/-}$ *mTR*$^{+/-}$ mice appear grossly normal, both sexes weigh consistently less than wt littermates (see Fig. S1 in the supplemental material). With increasing age, *Pot1b*$^{-/-}$ *mTR*$^{+/+}$ and *Pot1b*$^{-/-}$ *mTR*$^{+/-}$ mice developed hyperpigmentation around their tails, legs, paws, and snout, which was never observed in wt littermates (Fig. 2A and data not shown). Nail dystrophy was also prominent in both groups (see Fig. S3A in the supplemental material). The reduction in body weight, hyperpigmentation, and nail dystrophy were all more pronounced in *Pot1b*$^{-/-}$ *mTR*$^{+/-}$ mice, suggesting that phenotypes observed in *Pot1b*$^{-/-}$ *mTR*$^{+/+}$ mice are enhanced in the setting of telomerase deficiency. In agreement with this observation, testicular atrophy and germ cell depletion were more severe in age-matched *Pot1b*$^{-/-}$*mTR*$^{+/-}$ mice, with a threefold decrease in testicular volume and nearly complete absence of all stages of spermatogenesis by 170 days of age (Fig. 2A; see also Fig. S2B and C in the supplemental material). However, the markedly decreased cellularity in these tubules yielded a falsely low number of TUNEL-positive cells (Fig. 2A and B). *Pot1b*$^{-/-}$ *mTR*$^{+/-}$ mice also exhibited a ~25-fold increase in the number of TUNEL-positive apoptotic bodies in intestinal crypts (Fig. 2A and C), and this increase in apoptosis was paralleled by a corresponding increase in the anaphase bridge index, a hallmark of telomere dysfunction (Fig. 2D; see also Fig. S3B in the supplemental material) (6, 40). Consistent with the observation that cells with dysfunctional telomeres activate the p53-dependent p21-signaling pathway, immunohistochemical staining revealed abundant p21-positive cells in intestinal epithelium from *Pot1b*$^{-/-}$ *mTR*$^{+/-}$ intestines (Fig. S3B in the supplemental material). In contrast, no anaphase bridges or p21 staining was observed in *Pot1b*$^{-/-}$ *mTR*$^{+/+}$ intestines (Fig. 2D; see also Fig. S3B in the supplemental material). The *Pot1b*$^{-/-}$ *mTR*$^{-/-}$ mouse, in the context of its young age (13 days), yielded the most severe proliferative defects in all organs examined, including nearly complete absence of germ cells representing all stages of spermatogenesis, increased intestinal apoptosis, and p21 staining (Fig. 2A and B; see also Fig. S3B in the supplemental material). These results suggest that telomerase deficiency greatly exacerbated proliferative defects observed in *Pot1b*$^{-/-}$ animals.

Effect of Pot1b loss and telomerase deficiency on the hematopoietic system. Compared to wt and *Pot1b*$^{-/-}$ *mTR*$^{+/+}$ mice, *Pot1b*$^{-/-}$ *mTR*$^{+/-}$ mice have a life span that is significantly short, with an overall median life span of 180 days (Fig. 3A). Female *Pot1b*$^{-/-}$ *mTR*$^{+/-}$ mice were significantly more adversely impacted than males (median life span of 84 days for females and 196 days for males). While all *Pot1b*$^{-/-}$ *mTR*$^{+/-}$ mice have normal complete peripheral blood counts and profiles at 28 days of age, by 79 days of age female mice (~200 days for males) developed anemia (reduced RBC and hemoglobin counts), severe leukopenia (reductions in granulocytes, lymphocytes, monocytes, and eosinophils), and thrombocytopenia (reduction in platelets), while peripheral blood counts in age-matched *Pot1b*$^{-/-}$ *mTR*$^{+/+}$ mice showed normal trilineage hematopoiesis (Fig. 3B and data not shown). Sixty percent of all *Pot1b*$^{-/-}$ *mTR*$^{+/-}$ mice examined exhibited peripheral smears essentially devoid of leukocytes (Fig. 3C, frame a). Granulocytes that were present were left-shifted with dysplastic features, and immature blasts were present (Fig. 3C, frames b to d). The *Pot1b*$^{-/-}$ *mTR*$^{-/-}$ mouse also exhibited severe pancytopenia with dysplastic erythrocytes and granulocytes with morphological features suggestive of an evolving myelodysplastic syndrome (MDS) (Fig. 3B). FACS analysis with annexin V and 7-AAD showed an eightfold increase in the number of apoptotic cells (Fig. 3D). These results suggest that the leukopenia observed in *Pot1b*$^{-/-}$ *mTR*$^{+/-}$ and *Pot1b*$^{-/-}$ *mTR*$^{-/-}$ mice is a result of increased apoptosis, in agreement with the elevated level of apoptosis observed in other proliferative tissue compartments including the testes and the gastrointestinal track.

Histological examination of femurs and sternums from *Pot1b*$^{-/-}$ *mTR*$^{+/-}$ mice revealed that BM displayed a striking absence of trilineage hematopoiesis, which was almost completely replaced by stromal adipose tissues (Fig. 4A and data not shown). The *Pot1b*$^{-/-}$ *mTR*$^{-/-}$ mouse exhibited a similar degree of BM ablation, which was remarkable considering its young age (Fig. 4A). This severe BM failure is likely the cause of early demise. Using antibodies against CD11b (Mac-1) and Gr-1 to mark mature granulocytes, FACS analysis revealed an approximately fourfold reduction in this cell population in *Pot1b*$^{-/-}$ *mTR*$^{+/-}$ mice (Fig. 4B), correlating with the reduction in granulocytes determined by differential analysis of cytospin preparations (Fig. 4C and D). A twofold decrease in erythroids was also observed (Fig. 4D). The acute BM failure observed in *Pot1b*$^{-/-}$ *mTR*$^{+/-}$ and *Pot1b*$^{-/-}$ *mTR*$^{-/-}$ mice suggests that the survival potential of early hematopoietic progenitor and stem cells might be compromised. To test this hypothesis, we isolated BM from age-matched *Pot1b*$^{+/-}$ *mTR*$^{+/-}$ and *Pot1b*$^{-/-}$ *mTR*$^{+/-}$ mice and compared their abil-

of testes sections. (Fourth row) Hematoxylin and eosin staining of sections of intestinal sections. Arrows indicate apoptotic nuclei. (Fifth row) TUNEL staining of intestinal sections. Scale bars for all sections are 50 μm. (B) Quantitation of number of TUNEL-positive cells in testes from mice of the indicated genotypes. A minimum of 780 seminiferous tubules was examined per genotype ($n = 3$ mice per genotype; average age, 215 days, except for the single 13-day-old *Pot1b*$^{-/-}$ *mTR*$^{-/-}$ mouse). Error bars represent standard error of the mean. *, $P < 0.01$; #, $P = 0.32$ (Student's *t* test). (C) Quantitation of the number of apoptotic bodies in the gastrointestinal track detected by TUNEL assay. A minimum of 1,200 crypts per genotype was examined ($n = 4$ mice per genotype; average age, 226 days). Error bars represent standard error of the mean. *, $P < 0.05$; **, $P < 0.01$ (Student's *t* test). (D) Quantitation of anaphase bridges in small intestines, with number of crypts analyzed as in panel C. Error bars represent standard error of the mean. **, $P < 0.01$ (Student's *t* test).

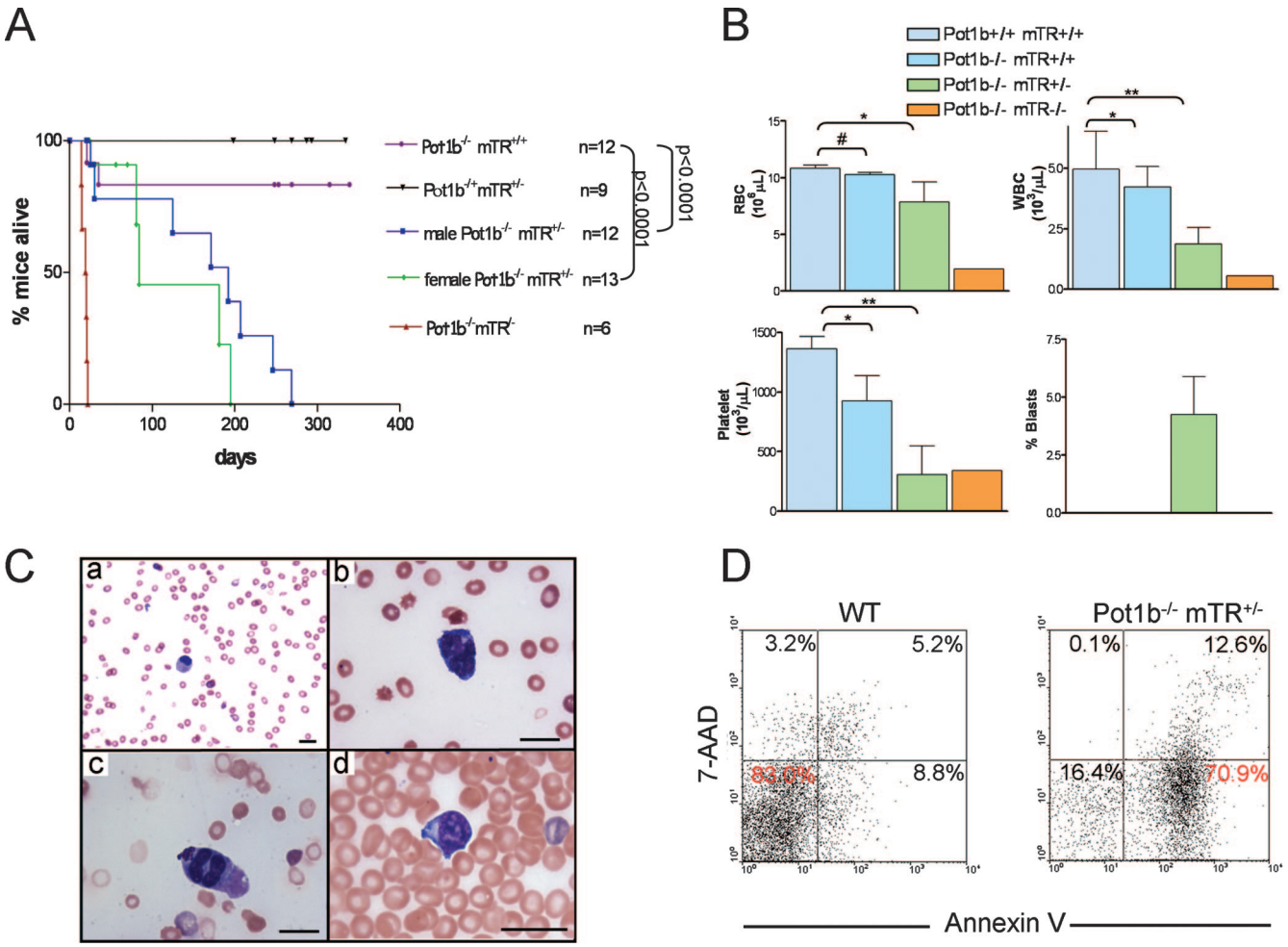

FIG. 3. Hematopoietic defects and premature death in *Pot1b*$^{-/-}$ *mTR*$^{+/-}$ and *Pot1b*$^{-/-}$ *mTR*$^{-/-}$ mice. (A) Kaplan-Meier survival analysis of *Pot1b*$^{+/-}$ *mTR*$^{+/-}$ intercross. For clarity, not all genotypes generated are shown. (B) Peripheral blood counts (RBCs, white blood cells, platelets, and immature blasts) of mice of the indicated genotypes. *Pot1b*$^{-/-}$ *mTR*$^{+/-}$ female mice analyzed are between 28 and 48 days of age; males are between 180 and 240 days of age. Error bars represent standard error of the mean. #, $P = 0.54$; *, $P < 0.05$; **, $P < 0.01$ (Student's *t* test). (C, a) Pancytopenia with rare granulocytes. (b and c) Dysplastic granulocytes. (d) Immature blasts found in peripheral smears of *Pot1b*$^{-/-}$ *mTR*$^{+/-}$ mice. All scale markers are 20 μm. (D) 7-AAD/annexin-stained FACS profiles of wt and *Pot1b*$^{-/-}$ *mTR*$^{+/-}$ peripheral blood.

ities to generate CFU of myeloid cells including granulocytes, erythrocytes, monocytes, and megakaryocytes. As expected, total BM cells were significantly decreased in *Pot1b*$^{-/-}$ *mTR*$^{+/-}$ mice (Fig. 4E). Compared to *Pot1b*$^{+/-}$ *mTR*$^{+/-}$ controls, a striking decrease in both the size and number of colonies was observed in *Pot1b*$^{-/-}$ *mTR*$^{+/-}$ BM (Fig. 4F and data not shown). Taken together, these results suggest that renewal of hematopoietic progenitor/stem cells is severely compromised in *Pot1b*$^{-/-}$ *mTR*$^{+/-}$ and *Pot1b*$^{-/-}$ *mTR*$^{-/-}$ mice, likely resulting in a diminished life span.

Increased G-strand overhang and progressive telomere shortening in the absence of Pot1b. The increased global cellular proliferative defects observed in *Pot1b*$^{-/-}$ *mTR*$^{+/-}$ and *Pot1b*$^{-/-}$ *mTR*$^{-/-}$ mice suggest that in the absence of Pot1b, diminished levels of telomerase might be insufficient to fully protect telomeres. This would result in the activation of DDR pathways to initiate p53-dependent checkpoint responses that would compromise cell viability. To examine the impact of Pot1b loss on telomere length, genomic DNA isolated from wt and *Pot1b*$^{-/-}$ livers and kidneys was probed under native (nondenaturing) and denaturing conditions to detect the 3′ single-stranded G-rich overhang and total telomeres, respectively. An increase in the G-strand overhang was observed in liver and kidney DNA of all mice lacking *Pot1b*, while total telomere length was not appreciably altered (Fig. 5A and data not shown). To further examine the impact of *Pot1b* loss on telomere metabolism, we generated immortalized *Pot1b*$^{+/-}$ *mTR*$^{+/-}$, *Pot1b*$^{+/-}$ *mTR* $^{\text{lp;\&0.25q}>-/-}$, *Pot1b*$^{-/-}$ *mTR*$^{+/+}$, and *Pot1b*$^{-/-}$ *mTR*$^{+/-}$ MEFs and passaged them in vitro for several population doublings (PDs). Deletion of *Pot1b* resulted in an increase in the G-strand overhang, which diminished following treatment with exonuclease I, demonstrating that the single-stranded G-rich repeats originated from the 3′ end of telomeres (Fig. 5B; see also Fig. S4 in the supplemental material). Deletion of Pot1b also resulted in rapid loss of overall telomere length, which was further exacerbated in *Pot1b*$^{-/-}$ *mTR*$^{+/-}$ MEFs, suggesting that in the setting of Pot1b defi-

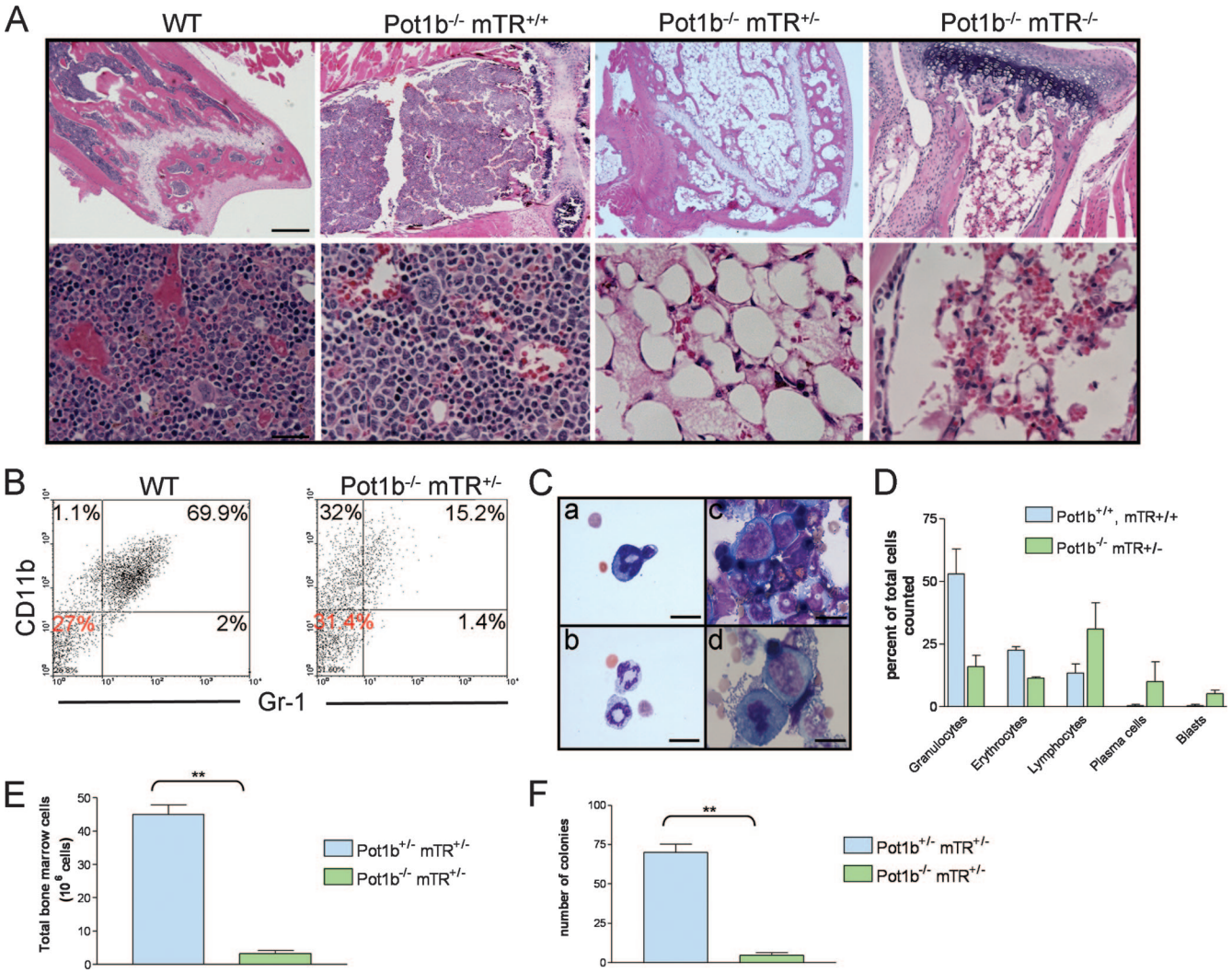

FIG. 4. BM ablation in *Pot1b*$^{-/-}$ *mTR*$^{+/-}$ and *Pot1b*$^{-/-}$ *mTR*$^{-/-}$ mice. (A) Hematoxylin and eosin staining of sections of femurs of mice of the indicated genotypes. For the ages of the mice analyzed, see the legend of Fig. 3. Scale bars: 500 μm (top), 50 μm (bottom). (B) CD11b/Gr-1 stained FACS profiles of wt and *Pot1b*$^{-/-}$ *mTR*$^{+/-}$ peripheral blood. (C) Cytospins of *Pot1b*$^{-/-}$ *mTR*$^{+/-}$ BM preparations showing dysplastic granulocytes (a and b) and blasts (c and d). Scale bar, 25 μm. (D) Differential of cell types found in BM cytospins from wt and *Pot1b*$^{-/-}$ *mTR*$^{+/-}$ mice. (E) Quantitation of total BM cells isolated from *Pot1b*$^{+/-}$ *mTR*$^{+/-}$ and *Pot1b*$^{-/-}$ *mTR*$^{+/-}$ mice. Values are averages from 3 mice (average age, 196 days). Error bars represent standard error of the mean. **, $P < 0.001$ (Student's *t* test). (F) Number of colonies from hematopoietic colony-forming assays. Sizes of BM-derived colonies using cells derived from *Pot1b*$^{+/-}$ *mTR*$^{+/-}$ and *Pot1b*$^{-/-}$ *mTR*$^{+/-}$ mice were assessed after 7 days of culture in semisolid medium. Mice age and number are as in panel E. Error bars represent standard error of the mean. **, $P < 0.0001$ (Student's *t* test).

ciency, telomerase haploinsufficiency accelerates telomere loss (Fig. 5B; see also Fig. S4 in the supplemental material).

Increased telomere attrition typically results in telomere dysfunction and the formation of end-to-end chromosomal fusions. Cytogenetic analyses revealed that while the number of fused chromosomes was minimal in *Pot1b*$^{-/-}$ *mTR*$^{+/-}$ MEFs at 10 PDs (0.3 fusions per metaphase), by 30 PDs the number of fused chromosomes increased to almost 2 per metaphase (Fig. 5C and E). Telomere fusions were also detectable by telomere restriction fragment (TRF)-Southern analysis, appearing at PD 35 and increasing in intensity by PD 41 (Fig. 5B, arrow). PNA-telomere FISH revealed that these end-to-end chromosomal fusions were Robertsonian-type p-p arm fusions without telomeres at the site of fusion (Fig. 5C). Quantitative telomere-FISH (qFISH) showed that *Pot1b*$^{-/-}$ *mTR*$^{+/-}$ MEFs at 30 PDs displayed a significant decrease in telomere length and a corresponding increase in the number of signal-free telomere ends (Fig. 5D), correlating with the global telomere attrition detected by TRF-Southern analysis. In contrast, despite accelerated telomere shortening detected by both TRF-Southern and qFISH analyses, *Pot1b*$^{-/-}$ *mTR*$^{+/+}$ MEFs did not exhibit an increase in the number of fused chromosomes with advanced passages (Fig. 5C and E).

The striking BM ablation phenotype observed in the *Pot1b*$^{-/-}$ *mTR*$^{+/-}$ mice prompted us to analyze cytogenetic profiles and telomere length in these mice. Compared to *Pot1b*$^{+/-}$ *mTR*$^{+/-}$ controls, *Pot1b*$^{-/-}$ *mTR*$^{+/-}$ primary BM and splenocytes exhibited increased numbers of fused chromo-

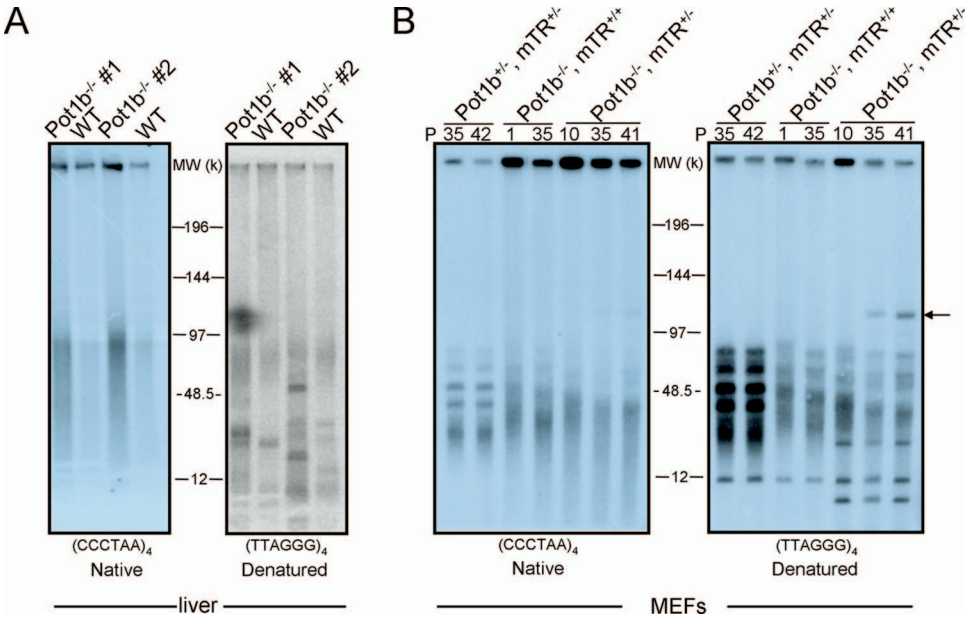

FIG. 5. Increased G overhang and telomere shortening in *Pot1b*$^{-/-}$ *mTR*$^{+/-}$ cells. (A) Genomic DNA purified from livers of 42-day-old wt and *Pot1b*$^{-/-}$ *mTR*$^{+/+}$ mice were digested with HinF1/RsaI and size fractionated. In-gel hybridization were performed under native conditions with a $(CCCTAA)_4$ probe to detect single-stranded telomeric DNA and subsequently under denaturing conditions with a $(TTAGGG)_4$ probe conditions to detect total telomeric DNA. (B) Genomic DNA isolated form MEFs of the indicated genotypes, and PDs were analyzed as in panel A. The arrow points to telomeric fusion products. (C) PNA-telomere FISH of metaphase spreads from MEFs of the indicated genotypes at PD 30. Arrows indicate end-to-end chromosomal fusions. (D) Quantitative-telomere FISH of MEFs in panel C. Mean telomere fluorescence units (TFUs) are shown, as well as the number of telomeres (*n*) analyzed. The arrow points to increased telomere signal-free ends. (E) Frequency of p-p arm chromosomal fusions with increasing PDs of MEFs with the indicated genotypes. Four samples per genotype were analyzed and a minimum of 35 metaphases per sample. Error bars represent standard error of the mean. (F) PNA-FISH of splenocytes derived from 200-day-old *Pot1b*$^{+/-}$ *mTR*$^{+/-}$ and *Pot1b*$^{-/-}$ *mTR*$^{+/-}$ mice. The arrow points to a fused chromosome. A minimum of 20 metaphases were analyzed. (G) qFISH of metaphases shown in panel F. The arrow points to increased telomere signal-free ends. (H) Number of fused chromosomes per metaphase of primary splenocytes and BM cells isolated from three 200- to 224-day-old *Pot1b*$^{+/-}$ *mTR*$^{+/-}$ and *Pot1b*$^{-/-}$ *mTR*$^{+/-}$ mice. Error bars represent standard error of the mean.

somes (Fig. 5F and H), significantly shortened telomere length, and increased numbers of signal-free ends as revealed by qFISH (Fig. 5G). Taken together, these results suggest that telomeres in highly proliferative tissues of *Pot1b*$^{-/-}$ *mTR*$^{+/-}$ mice are dysfunctional, resulting in end-to-end chromosomal fusions and subsequent breakage-fusion-bridge cycles that could activate a DDR that, depending on cell type, impinges upon the p53 pathway to elicit apoptosis and/or cellular senescence to reduce cellular proliferative capacity.

Deletion of both Pot1b and telomerase initiate an ATR-dependent DDR. We have previously shown that both Pot1a and Pot1b bind to the 3′ G-rich overhang to repress an ATR-mediated DDR at telomeres (12). Given that Pot1a by itself appears to be able to protect telomeres from activating ATR (8), we asked whether Pot1b is required to repress ATR activation at telomeres in the setting of telomerase deficiency. We monitored phosphorylated ATR levels in *Pot1b*$^{+/-}$ *mTR*$^{-/-}$ primary MEFs stably expressing vector or shPot1b shown previously to efficiently delete Pot1b (Fig. 6A) (12). Phosphorylated ATR and upregulation of p53 and p21 were observed in *Pot1b*$^{+/-}$ *mTR*$^{-/-}$ MEFs expressing shPot1b but not in the vector control (Fig. 6A). Consistent with the activation of a p53-p21 signaling pathway, depletion of Pot1b in *Pot1b*$^{+/-}$ *mTR*$^{-/-}$ primary MEFs also resulted in growth suppression, while no growth defect was observed in vector-infected MEFs (Fig. 6B). These results suggest that even though Pot1a is present on telomeres at wt levels, Pot1b is required to prevent the activation of an ATR-dependent DDR in the setting of telomerase deficiency. This result correlates well with our in vivo data, suggesting that telomeres become dysfunctional when both telomerase and Pot1b functions are abrogated, initiating apoptosis and/or growth arrest in highly proliferative tissues.

We next asked whether telomerase itself plays an active role in preventing a DDR at telomeres in the absence of Pot1b. Telomerase has been postulated to have a capping function that may function to modulate the DDR independent of its role in telomere maintenance (25, 45). To test whether Pot1b requires telomerase to protect telomeres, we monitored phosphorylated ATR levels in *Pot1b*$^{+/-}$ *mTR*$^{+/-}$, *Pot1b*$^{-/-}$ *mTR*$^{+/-}$, and *Pot1b*$^{-/-}$ *mTR*$^{+/+}$ immortalized MEFs expressing vector or shRNA targeting Tert (shTert) to knock down *mTert*. RT-PCR analysis demonstrated that *mTert* was efficiently depleted in shTert-infected cells (Fig. 6C). As expected, vector-treated *Pot1b*$^{-/-}$ *mTR*$^{+/-}$ MEFs display robust ATR phosphorylation. A low level of ATR phosphorylation was also observed in vector-treated *Pot1b*$^{-/-}$ *mTR*$^{+/+}$ MEFs, suggesting the presence of some dysfunctional telomeres in cells lacking Pot1b. Correlating with an elevated DDR in *Pot1b*$^{-/-}$ *mTR*$^{+/-}$ MEFs, γ-H2AX and 53BP1-positive telomere dysfunction-induced DNA damage foci (TIFs) were observed in these cells (Fig. 6D and data

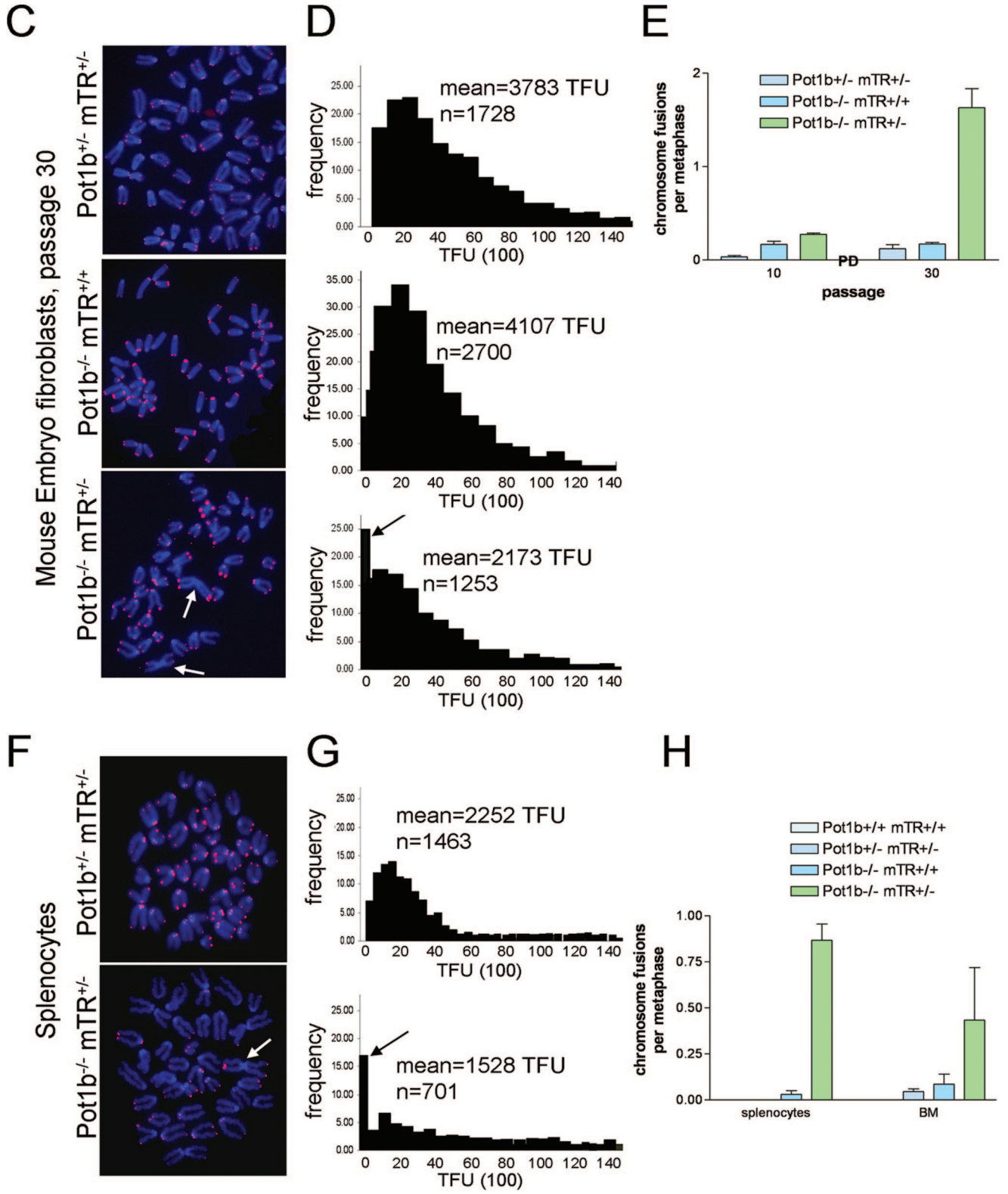

FIG. 5—*Continued.*

not shown) although at a much lower frequency than those observed when Pot1a was deleted (12, 41). Interestingly, we were not able to detect TIFs in *Pot1b*$^{-/-}$ *mTR*$^{+/+}$ MEFs despite the presence of low levels of phosphorylated ATR (Fig. 6D). Finally, acute depletion of *mTert* did not markedly affect the level of ATR phosphorylation in *Pot1b*$^{-/-}$ *mTR*$^{+/-}$ or *Pot1b*$^{-/-}$ *mTR*$^{+/+}$ MEFs (Fig. 6C). Taken together, our results suggest that in the absence of Pot1b,

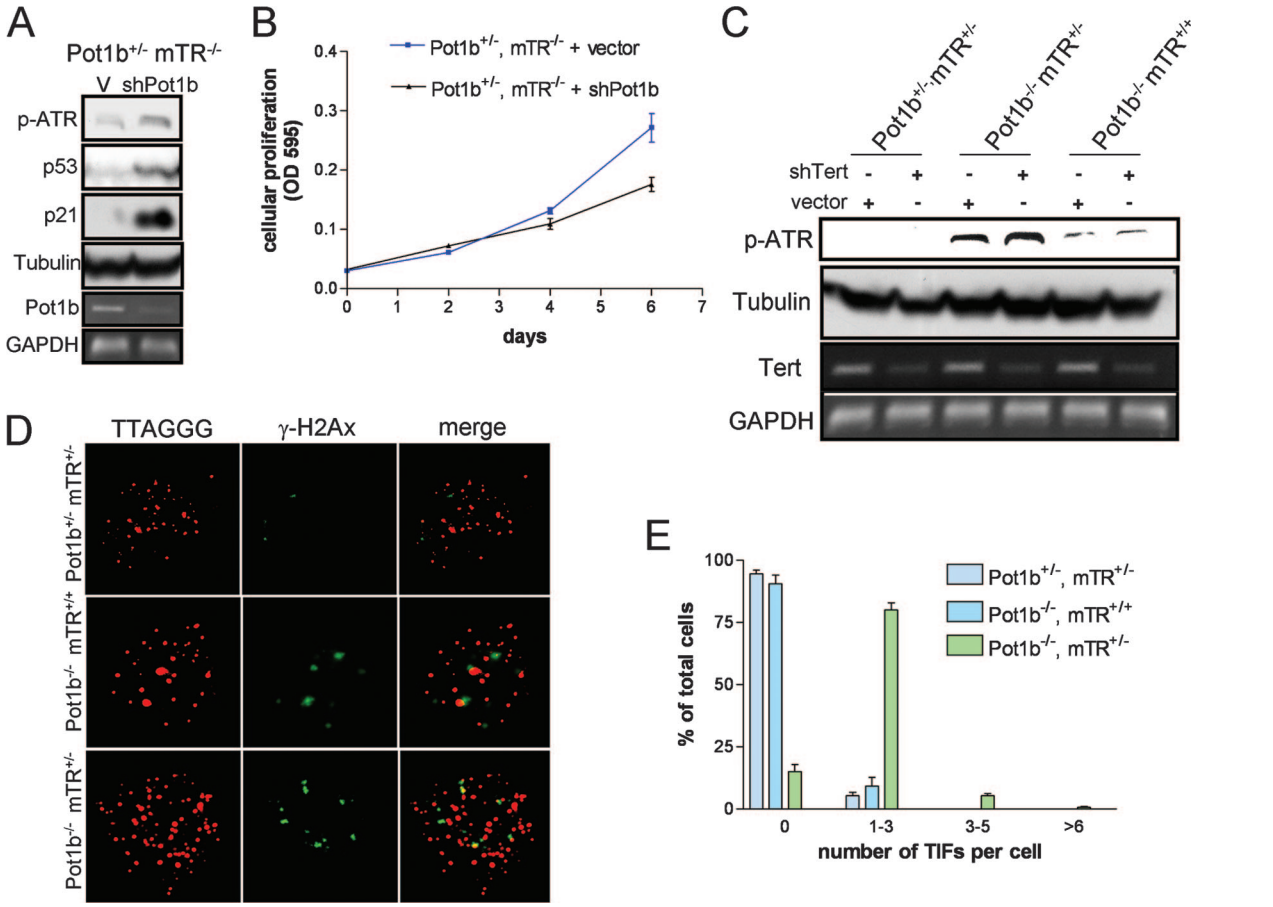

FIG. 6. *Pot1b* loss and telomerase deficiency initiates an ATR-dependent DNA damage response at telomeres. (A) Deletion of Pot1b in the absence of telomerase initiates ATR phosphorylation (p-ATR). Immortalized $Pot1b^{+/-}$ $mTR^{-/-}$ MEFs were infected with control vector or shRNA targeting Pot1b. Efficient *Pot1b* knockdown, as indicated by RT-PCR, induced ATR phosphorylation and upregulation of p53 and p21. Tubulin served as a protein loading control, and GAPDH (glyceraldehyde-3-phosphate dehydrogenase) served as an mRNA loading control. (B) Diminished cell proliferation upon deletion of Pot1b. Early passage (P2) primary $Pot1b^{+/-}$ $mTR^{-/-}$ MEFs were infected with control vectors or shPot1b and subjected to puromycin selection. Subsequently, cell numbers were measured at the indicated time points, with day 0 representing the first day after puromycin selection. Error bars represent standard error of the mean. (C) Minimal impact of ATR phosphorylation when telomerase is acutely deleted in the setting of Pot1b loss. Immortalized MEFs of the indicated genotypes were treated with vector control or shTert and monitored for phosphorylated ATR levels. Tubulin served as a protein loading control, and GAPDH served as an mRNA loading control. (D) Deletion of *Pot1b* and telomerase heterozygocity results in TIF formation. Immortalized MEFs of the indicated genotypes were analyzed by telomere PNA-FISH (red) and with antibody to γ-H_2AX (green) to detect TIFs. The images were merged to evaluate colocalization. Representative images are shown. (E) Quantitation of percentage of cells with γ-H_2AX-positive TIFs in MEFs of the indicated genotypes. A minimum of 250 nuclei were scored per genotype. Error bars represents standard error of the mean. OD 595, optical density at 595 nm.

telomeres become dysfunctional even when telomerase is present. This degree of dysfunction is enhanced when the telomerase level is reduced, resulting in the activation of a robust ATR-dependent DDR. However, telomerase per se does not appear to markedly influence the DDR at telomeres even in the absence of Pot1b.

DISCUSSION

The data presented here indicate that deletion of *Pot1b* and limiting telomerase activity in the mouse adversely impact upon the long-term maintenance of diverse cell types with high rates of cellular proliferation. In the absence of *Pot1b*, telomerase haploinsufficiency results in accelerated telomere shortening to generate dysfunctional telomeres that activate an ATR-dependent DDR, manifested in vivo as depletion of male germ and intestinal crypt cells, progressive BM failure, and premature death. Deletion of both *Pot1b* and telomerase results in early lethality, likely as a result of complications due to complete BM ablation. In addition to the severe compromise of highly proliferative tissues, $Pot1b^{-/-}$ $mTR^{+/-}$ mice also exhibit hyperpigmentation and nail dystrophy. These results indicate an essential role for Pot1b in the maintenance of genome integrity and long-term viability of proliferative tissues in the setting of telomerase deficiency.

***Pot1b*$^{-/-}$ *mTR*$^{+/-}$ mouse as a model for DC.** The phenotypes observed in the $Pot1b^{-/-}$ $mTR^{+/-}$ mouse suggest that it faithfully models most, if not all, aspects of DC. DC is an inherited multisystem disorder of stem cell failure characterized by the clinical triad of skin hyperpigmentation, nail dystrophy, and mucosal leukoplakia (reviewed in reference 10).

Increasing evidence suggests that DC is a disease of accelerated telomere shortening. The X-linked form of this disease is due to mutations in DKC1 that affect dyskerin expression, a ribonucleoprotein involved in processing of *hTERC* (15, 39), while the autosomal-dominant (AD) form of this disease stems from mutations in *hTERC* and *hTERT* (1, 32). An autosomal recessive form of this disease due to mutations in the telomerase-associated protein NOP-10 has been recently identified (35). The primary cause of premature death in these patients is due to progressive BM failure and complications stemming from marrow aplasia. Telomere shortening plays a causal role in the BM failure phenotype observed in the AD form of DC since hematopoietic stem cells from these patients show proliferative defects due to telomere dysfunction (11). In addition, DC families bearing mutations in *hTert* and *hTerc* show progressive telomere shortening with each generation and a disease anticipation phenotype consistent with telomerase haploinsufficiency (1, 5, 24, 34).

The availability of a mouse model that recapitulates the most important clinical phenotype of DC (BM failure) should result in therapeutic insights into this disease process. For example, our data suggest that *Pot1b*$^{-/-}$ *mTR*$^{+/-}$ hematopoietic stem cells display a profound reduction in colony forming potential due to increased apoptosis as a result of dysfunctional telomeres that activate a DDR to initiate p53-dependent apoptosis. Therefore, treatment of DC patients with immunosuppressive therapy is not predicted to be efficacious. Other options, including collection and storage of hematopoietic stem cells (HSCs) from mobilized peripheral blood for autologous transplantation, might also not be beneficial since it will be difficult to collect enough HSCs from DC patients for sufficient repopulation (11). To circumvent this difficulty, it might be possible in the future to overexpress telomerase in autologous HSCs from AD DC patients to correct for the intrinsic telomere defect.

DC is but one of several BM failure syndromes in which telomere dysfunction is implicated as a causal mechanism. Mutations in *hTerc* resulting in shortened telomeres have also been observed in aplastic anemia and MDS (33, 43, 44). In addition to BM failure, the *Pot1b*$^{-/-}$ *mTR*$^{+/-}$ mouse displays features consistent with MDS, including dysplasia of granulocytes and erythrocytes, cytogenetic abnormalities, and ineffective hematopoiesis in one or more lineages. It is therefore tempting to speculate that DC, aplastic anemia, and MDS are all part of a continuum of disorders that are due to defects in telomere metabolism. Since ~60% of all DC patients remain genetically uncharacterized, our results suggest that POT1, as well as other components of the shelterin complex, should be analyzed to discern the presence of destabilizing mutations that could result in telomere dysfunction. The presence of mutations in the shelterin protein TIN2 in patients with DC supports this notion (29, 36).

Mouse models of telomere shortening. The *mTR* knockout mouse validated the notion that proper maintenance of telomere length is essential for the maintenance of organs with high proliferative capacity (4, 19). While early generations of mTR null mice appear normal due to their large telomere reserve, highly proliferative tissues including germ and intestinal stem cells in late-generation *mTR*$^{-/-}$ mice exhibit impaired proliferation and/or increased apoptosis. However, despite critical telomere shortening, late-generation *mTR*$^{-/-}$ mice do not display overt symptoms of BM failure or other features of DC. Compared to the *mTR* null mice, the use of a CAST/EiJ strain haploinsufficient for telomerase activity resulted in enhanced telomere shortening and the development of a similar spectrum of cellular defects in highly proliferative organs (13). While BM stem cells from these mice display a reduced capacity to repopulate lethally irradiated recipients, CAST/EiJ *mTR*$^{+/-}$ mice also do not exhibit overt BM failure. Interestingly, phenotypes associated with aged, late-generation *mTR* null mice, including hair graying and alopecia, are not observed in *Pot1b*$^{-/-}$ *mTR*$^{+/-}$ mice. These results suggest the possibility that proliferative tissue compartments might be differentially sensitive to telomere dysfunction generated as a result of *Pot1b* loss and telomerase depletion. On the other hand, it is also likely that manifestation of hair graying and alopecia require additional aging simply not achievable in *Pot1b*$^{-/-}$ *mTR*$^{+/-}$ mice. Finally, since multiple generational matings are not required for *Pot1b*$^{-/-}$ *mTR*$^{+/-}$ mice to manifest proliferative defects, this mouse model should be useful to study the impact of additional genetic alterations in the background of accelerated telomere shortening (17).

Role of Pot1b in modulating C-strand resection and the ATR-dependent DDR. Our data indicate that deletion of *Pot1b* results in dramatic 3′ G-rich overhang elongation and a telomere shortening phenotype that is further exacerbated by telomerase haploinsufficiency. Since this increase in the 3′ overhang occurs in the absence of telomerase activity (16), we speculate that Pot1b functions primarily in the control of nucleolytic processing of the 5′ C-rich strand by regulating nucleolytic processing from an as yet unidentified nuclease(s), leading to unregulated degradation of the C strand and concomitant increase in the G strand. Given the rapidity of telomere shortening in the absence of Pot1b, the rate of C-strand degradation must exceed the rate of telomere addition by telomerase. Paradoxically, despite the accelerated telomere shortening observed in the absence of *Pot1b*, chromosomal fusions and TIFs were not prevalent in late-passage *Pot1b* null MEFs. These results suggest that deletion of *Pot1b* does not activate a robust DDR at telomeres, a notion confirmed by the observations that ATR is only minimally phosphorylated in *Pot1b*$^{-/-}$ MEFs and that anaphase bridges and p21 upregulation in intestines of *Pot1b*$^{-/-}$ mice are absent. However, the presence of extensive germ cell depletion argues that some form of telomere dysfunction that activates a proliferative checkpoint must be present in *Pot1b* null mice. Taken together, our results suggest that Pot1a is insufficient to fully protect telomeres from engaging an ATR-dependent DDR at telomeres but that both proteins are required for full protection. It will be interesting to determine whether the increased germ cell apoptosis observed in *Pot1b*$^{-/-}$ mice requires the presence of an intact p53 pathway.

ACKNOWLEDGMENTS

We acknowledge the T. C. Tsu Molecular Cytogenetics Core for outstanding cytogenetic services (under grant NCI CA016672). S.C. acknowledges generous financial support from the Welch Foundation, the Elsa U. Pardee Foundation, the Abraham and Phyllis Katz Foundation, the Susan G. Koman for the Cure, and the Michael Kadoorie Cancer Genetic Research Program and support from the NIH (RO1AG02888 and RO1CA129037). Y.D. was supported by

1K01CA124461. M.J.Y. is supported by American Cancer Society's institutional research grant and University of Texas M. D. Anderson Cancer Center Physician Scientist Award.

REFERENCES

1. **Armanios, M., J. L. Chen, Y. P. Chang, R. A. Brodsky, A. Hawkins, C. A. Griffin, J. R. Eshleman, A. R. Cohen, A. Chakravarti, A. Hamosh, and C. W. Greider.** 2005. Haploinsufficiency of telomerase reverse transcriptase leads to anticipation in autosomal dominant dyskeratosis congenita. Proc. Natl. Acad. Sci. USA **102:**15960–15964.
2. **Baumann, P., and T. R. Cech.** 2001. Pot1, the putative telomere end-binding protein in fission yeast and humans. Science **292:**1171–1175.
3. **Baumann, P., E. Podell, and T. R. Cech.** 2002. Human Pot1 (protection of telomeres) protein: cytolocalization, gene structure, and alternative splicing. Mol. Cell. Biol. **22:**8079–8087.
4. **Blasco, M. A., H. W. Lee, M. P. Hande, E. Samper, P. M. Lansdorp, R. A. DePinho, and C. W. Greider.** 1997. Telomere shortening and tumor formation by mouse cells lacking telomerase RNA. Cell **91:**25–34.
5. **Cerone, M. A., R. J. Ward, J. A. Londoño-Vallejo, and C. Autexier.** 2005. Telomerase RNA mutated in autosomal dyskeratosis congenita reconstitutes a weakly active telomerase enzyme defective in telomere elongation. Cell Cycle **4:**585–589.
6. **Chang, S., A. S. Multani, N. G. Cabrera, M. L. Naylor, P. Laud, D. Lombard, S. Pathak, L. Guarente, and R. A. DePinho.** 2004. Essential role of limiting telomeres in the pathogenesis of Werner syndrome. Nat. Genet. **36:**877–882.
7. **Churikov, D., and C. M. Price.** 2008. Pot1 and cell cycle progression cooperate in telomere length regulation. Nat. Struct. Mol. Biol. **15:**79–84.
8. **Denchi, E. L., and T. de Lange.** 2007. Protection of telomeres through independent control of ATM and ATR by TRF2 and POT1. Nature **448**: 1068–10671.
9. **Deng, Y., S. S. Chan, and S. Chang.** 2007. Telomere dysfunction and tumour suppression: the senescence connection. Nat. Rev. Cancer **8:**450–458.
10. **Dokal, I.** 2000. Dyskeratosis congenita in all its forms. Br. J. Haematol. **110**:768–779.
11. **Goldman, F. D., G. Aubert, A. J. Klingelhutz, M. Hills, S. R. Cooper, W. S. Hamilton, A. J. Schlueter, K. Lambie, C. J. Eaves, and P. M. Lansdorp.** 2008. Characterization of primitive hematopoietic cells from patients with dyskeratosis congenita. Blood **111:**4523–4531.
12. **Guo, X., Y. Deng, Y. Lin, W. Cosme-Blanco, S. Chan, H. He, G. Yuan, E. J. Brown, and S. Chang.** 2007. Dysfunctional telomeres activate an ATM-ATR-dependent DNA damage response to suppress tumorigenesis. EMBO J. **26:**4709–4719.
13. **Hao, L. Y., M. Armanios, M. A. Strong, B. Karim, D. M. Feldser, D. Huso, and C. W. Greider.** 2005. Short telomeres, even in the presence of telomerase, limit tissue renewal capacity. Cell **123:**1121–1131.
14. **He, H., A. S. Multani, W. Cosme-Blanco, H. Tahara, J. Ma, S. Pathak, Y. Deng, and S. Chang.** 2006. POT1b protects telomeres from end-to-end chromosomal fusions and aberrant homologous recombination. EMBO J. **25:**5180–5190.
15. **Heiss, N. S., S. W. Knight, T. J. Vulliamy, S. M. Klauck, S. Wiemann, P. J. Mason, A. Poustka, and I. Dokal.** 1998. X-linked dyskeratosis congenita is caused by mutations in a highly conserved gene with putative nucleolar functions. Nat. Genet. **19:**32–38.
16. **Hockemeyer, D., J. P. Daniels, H. Takai, and T. de Lange.** 2006. Recent expansion of the telomeric complex in rodents: Two distinct POT1 proteins protect mouse telomeres. Cell **126:**63–77.
17. **Hockemeyer, D., W. Palm, R. C. Wang, S. S. Couto, and T. de Lange.** 2008. Engineered telomere degradation models dyskeratosis congenita. Genes Dev. **22**:1773–1785.
18. **Kelleher, C., I. Kurth, and J. Lingner.** 2005. Human protection of telomeres 1 (POT1) is a negative regulator of telomerase activity in vitro. Mol. Cell. Biol. **25:**808–818.
19. **Lee, H. W., M. A. Blasco, G. J. Gottlieb, J. W. Horner II, C. W. Greider, and R. A. DePinho.** 1998. Essential role of mouse telomerase in highly proliferative organs. Nature **392:**569–574.
20. **Lei, M., E. R. Podell, P. Baumann, and T. R. Cech.** 2003. DNA self-recognition in the structure of Pot1 bound to telomeric single-stranded DNA. Nature **426:**198–203.
21. **Lei, M., A. J. Zaug, E. R. Podell, and T. R. Cech.** 2005. Switching human telomerase on and off with hPOT1 protein in vitro. J. Biol. Chem. **280:** 20449–20456.
22. **Lewandoski, M., K. M. Wassarman, and G. R. Martin.** 1997. Zp3-Cre, a transgenic mouse line for the activation or inactivation of loxP-flanked target genes specifically in the female germ line. Curr. Biol. **7:**148–151.
23. **Loayza, D., and T. De Lange.** 2003. POT1 as a terminal transducer of TRF1 telomere length control. Nature **423:**1013–1018.
24. **Marrone, A., D. Stevens, T. Vulliamy, I. Dokal, and P. J. Mason.** 2004. Heterozygous telomerase RNA mutations found in dyskeratosis congenita and aplastic anemia reduce telomerase activity via haploinsufficiency. Blood **104:**3936–3942.
25. **Masutomi, K., R. Possemato, J. M. Wong, J. L. Currier, Z. Tothova, J. B. Manola, S. Ganesan, P. M. Lansdorp, K. Collins, and W. C. Hahn.** 2005. The telomerase reverse transcriptase regulates chromatin state and DNA damage responses. Proc. Natl. Acad. Sci. USA **102:**8222–8227.
26. **Palm, W., and T. de Lange.** 4 August 2008. How shelterin protects mammalian telomeres. Annu. Rev. Genet. doi:10.1146/annurev.genet.41.110306.130350.
27. **Raices, M., R. E. Verdun, S. A. Compton, C. I. Haggblom, J. D. Griffith, A. Dillin, and J. Karlseder.** 2008. *C. elegans* telomeres contain G-strand and C-strand overhangs that are bound by distinct proteins. Cell **132:**745–757.
28. **Rudolph, K. L., S. Chang, H. W. Lee, M. Blasco, G. J. Gottlieb, C. Greider, and R. A. DePinho.** 1999. Longevity, stress response, and cancer in aging telomerase-deficient mice. Cell **96:**701–712.
29. **Savage, S. A., N. Giri, G. M. Baerlocher, N. Orr, P. M. Lansdorp, and B. P. Alter.** 2008. TINF2, a component of the shelterin telomere protection complex, is mutated in dyskeratosis congenita. Am. J. Hum Genet. **82:**501–509.
30. **Shakirov, E. V., Y. V. Surovtseva, N. Osbun, and D. E. Shippen.** 2005. The *Arabidopsis* Pot1 and Pot2 proteins function in telomere length homeostasis and chromosome end protection. Mol. Cell. Biol. **25:**7725–7733.
31. Reference deleted.
32. **Vulliamy, T., A. Marrone, F. Goldman, A. Dearlove, M. Bessler, P. J. Mason, and I. Dokal.** 2001. The RNA component of telomerase is mutated in autosomal dominant dyskeratosis congenita. Nature **413:**432–435.
33. **Vulliamy, T., A. Marrone, I. Dokal, and P. J. Mason.** 2002. Association between aplastic anaemia and mutations in telomerase RNA. Lancet **359:** 2168–2170.
34. **Vulliamy, T., A. Marrone, R. Szydlo, A. Walne, P. J. Mason, and I. Dokal.** 2004. Disease anticipation is associated with progressive telomere shortening in families with dyskeratosis congenita due to mutations in TERC. Nat. Genet. **36:**447–449.
35. **Walne, A. J., T. Vulliamy, A. Marrone, R. Beswick, M. Kirwan, Y. Masunari, F. H. Al-Qurashi, M. Aljurf, and I. Dokal.** 2007. Genetic heterogeneity in autosomal recessive dyskeratosis congenita with one subtype due to mutations in the telomerase-associated protein NOP10. Hum. Mol. Genet. **16:** 1619–1629.
36. **Walne, A. J., T. J. Vulliamy, R. Beswick, M. Kirwan, and I. Dokal.** 30 July 2008. TINF2 mutations result in very short telomeres: analysis of a large cohort of patients with dyskeratosis congenita and related bone marrow failure syndromes. Blood **112:**3594–3600. [Epub ahead of print.]
37. **Wang, F., E. R. Podell, A. J. Zaug, Y. Yang, P. Baciu, T. R. Cech, and M. Lei.** 2007. The POT1-TPP1 telomere complex is a telomerase processivity factor. Nature **445:**506–510.
38. **Wei, C., and C. M. Price.** 2004. Cell cycle localization, dimerization, and binding domain architecture of the telomere protein cPot1. Mol. Cell. Biol. **24:**2091–2102.
39. **Wong, J. M., and K. Collins.** 2006. Telomerase RNA level limits telomere maintenance in X-linked dyskeratosis congenita. Genes Dev. **20:**2848–2858.
40. **Wong, K. K., R. S. Maser, R. M. Bachoo, J. Menon, D. R. Carrasco, Y. Gu, F. W. Alt, and R. A. DePinho.** 2003. Telomere dysfunction and Atm deficiency compromises organ homeostasis and accelerates ageing. Nature **421:** 643–648.
41. **Wu, L., A. S. Multani, H. He, W. Cosme-Blanco, Y. Deng, J. M. Deng, O. Bachilo, S. Pathak, H. Tahara, S. M. Bailey, Y. Deng, R. R. Behringer, and S. Chang.** 2006. Pot1 deficiency initiates DNA damage checkpoint activation and aberrant homologous recombination at telomeres. Cell **126:**49–62.
42. **Xin, H., D. Liu, M. Wan, A. Safari, H. Kim, W. Sun, M. S. O'Connor, and Z. Songyang.** 2007. TPP1 is a homologue of ciliate TEBP-beta and interacts with POT1 to recruit telomerase. Nature **445:**559–562.
43. **Yamaguchi, H., G. M. Baerlocher, P. M. Lansdorp, S. J. Chanock, O. Nunez, E. Sloand, and N. S. Young.** 2003. Mutations of the human telomerase RNA gene (TERC) in aplastic anemia and myelodysplastic syndrome. Blood **102:** 916–918.
44. **Yamaguchi, H., R. T. Calado, H. Ly, S. Kajigaya, G. M. Baerlocher, S. J. Chanock, P. M. Lansdorp, and N. S. Young.** 2005. Mutations in TERT, the gene for telomerase reverse transcriptase, in aplastic anemia. N. Engl. J. Med. **352:**1413–1424.
45. **Zhu, J., H. Wang, J. M. Bishop, and E. H. Blackburn.** 1999. Telomerase extends the lifespan of virus-transformed human cells without net telomere lengthening. Proc. Natl. Acad. Sci. USA **96:**3723–3728.